Alternative Normalized-Preconditioning for Scalable Iterative Large-MIMO Detection

Jiuyu Liu, Yi Ma, and Rahim Tafazolli

5GIC and 6GIC, Institute for Communication Systems, University of Surrey, Guildford, UK, GU2 7XH

Emails: (jiuyu.liu, y.ma, r.tafazolli)@surrey.ac.uk

Abstract—Signal detection in large multiple-input multiple-output (large-MIMO) systems presents greater challenges compared to conventional massive-MIMO for two primary reasons. First, large-MIMO systems lack favorable propagation conditions as they do not require a substantially greater number of service antennas relative to user antennas. Second, the wireless channel may exhibit spatial non-stationarity when an extremely large aperture array (ELAA) is deployed in a large-MIMO system. In this paper, we propose a scalable iterative large-MIMO detector named ANPID, which simultaneously delivers *1)* close to maximum-likelihood detection performance, *2)* low computational-complexity (i.e., square-order of transmit antennas), *3)* fast convergence, and *4)* robustness to the spatial non-stationarity in ELAA channels. ANPID incorporates a damping demodulation step into stationary iterative (SI) methods and alternates between two distinct demodulated SI methods. Simulation results demonstrate that ANPID fulfills all the four features concurrently and outperforms existing low-complexity MIMO detectors, especially in highly-loaded large-MIMO systems.

I. INTRODUCTION

In forthcoming wireless communication paradigms, large multiple-input multiple-output (large-MIMO) system will play an important role for serving a large number of user devices [1]. For instance, within the framework of smart city infrastructures, there will be hundreds or even thousands internet-of-things (IoT) devices. Therefore, compared to conventional massive-MIMO systems, the receiver design for large-MIMO systems presents unique challenges for two main reasons. First, large-MIMO systems do not require a substantially larger number of service antennas compared to user antennas, which implies that the favorable propagation assumption cannot be ensured [2]. Second, when an extremely large aperture array (ELAA) is incorporated into the system, the wireless channel can become spatially non-stationary [3]. Developing a scalable large-MIMO detector necessitates addressing the following requirements simultaneously: *1)* low computational-complexity, *2)* near-optimal performance, *3)* fast convergence, and *4)* robustness to the channel spatial non-stationarity [4], [5]. Current MIMO detectors can be categorized as either linear or nonlinear, based on their detection performance.

Linear MIMO detectors, such as minimum mean square error (LMMSE) and zero-forcing (ZF), are two of the most well-known detectors in the literature [5]. These detectors can achieve near-optimal performance when the MIMO channel is well-conditioned [6]. However, they both require a channel matrix inverse with cubic-order complexity of the user-antenna number, limiting their scalability. To address this issue, re-

searchers have proposed several types of iterative methods, mainly including stationary iterative (SI) methods, gradient descent methods, quasi-Newton methods, and belief propagation. Although these methods have scalable complexities, their detection performances become too sub-optimal when the system load is high since they can only converge to the performance of ZF/LMMSE [7].

Nonlinear MIMO detectors comprise various search-based approaches [4], such as maximum likelihood sequence detection (MLSD), likelihood ascent search, sphere decoding, K-best search, tabu search, and etc. While these detectors can potentially achieve (near-) MLSD performance, their complexities render them impractical, particularly for a large number of user antennas or high modulation orders [5]. Recently, several MIMO detectors based on alternating direction method of multipliers (ADMM) framework have been proposed to solve the MLSD problem subject to constraints [8]–[12], such as penalty-sharing ADMM (PS-ADMM). In comparison to linear detectors, ADMM-based methods provide significant performance gains in symmetric large-MIMO systems with stationary channels. However, these methods all involve the inversion or decomposition of a Gram matrix, which limits their scalability with user antennas.

In this paper, we propose a nonlinear MIMO detector called Alternative Normalized-Preconditioning for Iterative large-MIMO Detection (ANPID). Drawing inspiration from ADMM-based methods, our approach involves performing demodulation of three SI methods at each iteration: Jacobi iteration, Gauss-Seidel (GS) method, and symmetric successive over-relaxation (SSOR). Then, a damping step is developed to combine the estimation and demodulation vectors. Although GS and SSOR converge faster than Jacobi iteration, the signal power is not normalized in their iterative processes, which is inconsistent with the demodulation step. To address this issue, a well-designed diagonal matrix is proposed to normalized the signal power. Finally, the normalized GS/SSOR and Jacobi methods are alternately employed to achieve both fast convergence and close-to-MLSD performance.

The complexity of ANPID is comparable to that of SI methods, featuring scalable complexity, i.e., square-order of user-antenna number, as the projection and damping steps entail negligible complexities. Moreover, our simulation results demonstrate that ANPID achieves fast convergence and near-MLSD performance, even in highly-loaded and spatially-non-stationary large-MIMO systems.

II. SIGNAL MODEL, PRELIMINARIES AND PROBLEM STATEMENT

A. Signal Model

Let M and N denote the number of service and user antennas, respectively. The uplink signal model of large-MIMO systems can be represented as follows

$$\mathbf{y} = \mathbf{Hx} + \mathbf{v}, \tag{1}$$

where $\mathbf{y} \in \mathbb{C}^{M \times 1}$ stands for the received signal vector, $\mathbf{H} \in \mathbb{C}^{M \times N}$ for the random channel matrix, $\mathbf{x} \in \mathbb{C}^{N \times 1}$ for the transmitted signal vector, $\mathbf{v} \sim \mathcal{CN}(0, \sigma_v^2 \mathbf{I}_M)$ for the additive white Gaussian noise (AWGN), and $\mathbf{I}_M$ for an $(M) \times (M)$ identity matrix. Each element of $\mathbf{x}$ is assumed to be drawn from a modulation constellation $\mathcal{A}$ with equal probability, and fulfills: $\mathbb{E}\{\mathbf{x}\} = \mathbf{0}$; $\mathbb{E}\{\mathbf{xx}^H\} = \sigma_x^2 \mathbf{I}_N$. The following two random distributions of $\mathbf{H}$ are considered in this paper:

1) WSSUS channel: In conventional MIMO systems, the wireless channel is typically assumed to be wide-sense stationary uncorrelated scattering (WSSUS) [13], where each element of $\mathbf{H}$ obeys independent and identically distributed (i.i.d.) Rayleigh fading as follows

$$h_{m,n} \sim \mathcal{CN}\left(0, \sigma_h^2\right), \ \forall m, n, \tag{2}$$

where σ_h^2 denote the variance of every channel element.

2) ELAA channel: The wireless channel may become spatially non-stationary when an ELAA is deployed in an large-MIMO system. It is more appropriate to use a spherical-wave model to describe the spatial non-stationarity as follows [14]

$$h_{m,n}^{\text{ELAA}} = \varepsilon_{m,n} \left(\frac{\alpha}{d_{m,n}^\beta}\right) h_{m,n}, \tag{3}$$

where $\varepsilon_{m,n} \sim \mathcal{LN}(0, \sigma_s)$ stands for the log-normal distributed shadowing effects, α for the path-loss coefficients, β for the path-loss exponents and $d_{m,n}$ for the distance between the mth service and n^{th} user antennas. The correlation of $\varepsilon_{m,n}$ is characterized by exponentially decaying window in [3].

B. Preliminaries

Denote $\mathbf{x}_{\text{ML}}$ as the decision of MLSD, it can be determined by solving the following integer least squares problem

$$\mathbf{x}_{\text{ML}} = \underset{\mathbf{x} \in \mathcal{A}^N}{\arg\min} \|\mathbf{y} - \mathbf{Hx}\|^2, \tag{4}$$

where $\|\cdot\|$ denotes the Euclidean norm. However, it is computationally prohibitive to obtain $\mathbf{x}_{\text{ML}}$ for large value of N. As a lower-complexity alternative, several linear MIMO detectors (e.g., ZF and LMMSE) have been proposed. Their decision vectors, denoted by $\mathbf{x}_{\text{LIN}}$, can be expressed as follows

$$\mathbf{x}_{\text{LIN}} = \Gamma(\mathbf{A}^{-1}\mathbf{b}), \tag{5}$$

where $\mathbf{A} \triangleq \mathbf{H}^H\mathbf{H} + \rho\mathbf{I}_N$, $\mathbf{b} \triangleq \mathbf{H}^H\mathbf{y}$ and $\Gamma(\cdot)$ performs symbol-by-symbol decision. Specifically, the detector in (5) becomes ZF when the regularization factor $\rho = 0$, and LMMSE when $\rho = \sigma_v^2/\sigma_s^2$. However, due to the inversion of

$\mathbf{A}$, their complexities are still not scalable as N increases. SI methods are proposed to bypass the matrix inverse as follows

$$\mathbf{s}_t = \mathbf{s}_{t-1} + \mathbf{M}^{-1}(\mathbf{b} - \mathbf{As}_{t-1}), \tag{6}$$

where $t \geq 1$ denotes the iteration index, $\mathbf{s}_t$ the tth estimation vector, and $\mathbf{M}$ is the preconditioning matrix to distinguish between different SI methods. For examples, $\mathbf{M}_{\text{Jacobi}} = \mathbf{D}$, $\mathbf{M}_{\text{GS}} = \mathbf{D} + \mathbf{L}$ [15], and $\mathbf{M}_{\text{SSOR}} = (\mathbf{D} + \mathbf{L})\mathbf{D}^{-1}(\mathbf{D} + \mathbf{L})^H$ [16], where $\mathbf{D}$ and $\mathbf{L}$ are the diagonal and strict lower triangular parts of $\mathbf{A}$, respectively.

C. Problem Statement

In future large-MIMO systems, highly loaded situations will become increasingly common, and the wireless channels may exhibit spatially non-stationary. In Section I and II-B, existing MIMO detectors are discussed. Linear detectors are only effective when $N \ll M$, while nonlinear detectors have high computational-complexity, i.e., $\mathcal{O}(N^3)$ or more. To address these challenges, there is a pressing need for an advanced iterative large-MIMO detector that can satisfy the following key requirements simultaneously: *1)* close-to-MLSD performance even in highly loaded systems, *2)* low computational-complexity, i.e., $\mathcal{O}(N^2)$ or less, *3)* fast convergence, and *4)* robustness to channel spatial non-stationarity.

III. THE DEVELOPMENT OF ANPID METHOD

In this section, we will provide a details of developing ANPID. This involves integrating a damping demodulation step into SI methods, determining the optimal damping factor, designing normalized-SI techniques, and examining an alternative method on normalized-SI approaches. Furthermore, pseudocode for the implementation of ANPID will be provided.

A. Damping Demodulation for SI Methods

Inspired by the demodulation step in ADMM-based methods, we propose incorporating a demodulation process after SI methods. Additionally, a damping mechanism is introduced to combine the estimation and decision vectors as follows

$$\mathbf{s}_t = \mathbf{d}_{t-1} + \mathbf{M}^{-1}(\mathbf{b} - \mathbf{Ad}_{t-1}), \tag{7a}$$

$$\mathbf{x}_t = \Gamma(\mathbf{s}_t), \tag{7b}$$

$$\mathbf{d}_t = \omega_t \mathbf{d}_{t-1} + (1 - \omega_t)\mathbf{x}_t, \tag{7c}$$

where $\mathbf{x}_t$, ω_t and $\mathbf{d}_t$ denote the decision vector, damping factor, and damping vector, respectively. As with any iterative method, selecting an appropriate value of ω_t is crucial for achieving fast convergence and good detection performance.

Theorem 1: Given $\mathbf{H}$, $\mathbf{y}$, $\mathbf{x}_t$ and $\mathbf{d}_{t-1}$, the follow expression of ω_t minimizes the Euclidean distance between the received signal vector $\mathbf{y}$ and the damping vector $\mathbf{d}_t$

$$\omega_t = \frac{\Re\left(\boldsymbol{\nu}_t^H \boldsymbol{\tau}_t\right)}{\|\boldsymbol{\nu}_t\|^2}, \tag{8}$$

where $\boldsymbol{\tau}_t = \mathbf{y} - \mathbf{Hx}_t$ and $\boldsymbol{\nu}_t = \mathbf{Hd}_{t-1} - \mathbf{Hx}_t$, and $\Re(\cdot)$ outputs the real part of the input vector.
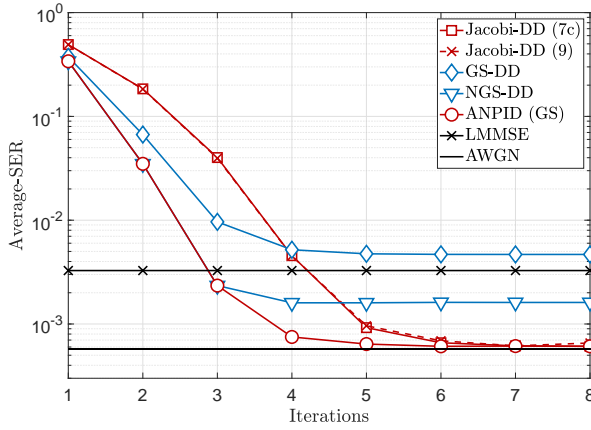
Proof: See Appendix A. ∎

Fig. 1. SER versus iteration of different algorithms in i.i.d. Rayleigh fading channel. $M = 256$; $N = 64$; 16 QAM; Es/No = 18 dB.

Remark 1: The complexity of calculating ω_t using (8) is $\mathcal{O}(2MN)$. While this complexity is scalable, updating ω_t at every iteration is not necessary. Our simulation results (see Fig. 1) indicate that setting $\omega^\star = \omega_1$ for all iterations achieves nearly the same convergence rate and symbol error rate (SER). Consequently, (7c) can be replaced by

$$\mathbf{d}_t = \omega^\star \mathbf{d}_{t-1} + (1 - \omega^\star)\mathbf{x}_t, \tag{9}$$

More specifically, $\omega^\star$ can be expressed as follows

$$\omega^\star = 1 - \frac{\Re\left(\mathbf{y}^H \mathbf{H} \mathbf{x}_1\right)}{\|\mathbf{H}\mathbf{x}_1\|^2}, \tag{10}$$

which can be easily calculated by plugging $\mathbf{d}_0 = \mathbf{0}$ into (8). The SI methods that use (9) as the damping step are referred to as Jacobi-DD, GS-DD, and SSOR-DD, respectively.

In Fig. 1, the wireless channel is assumed to follow i.i.d. Rayleigh fading. The detection performance of Jacobi-DD is comparable to that of the AWGN-bound, suggesting that it can achieve close-to-MLSD performance as well. However, GS-DD falls into a sub-optimal point with poor SER, despite its initially faster convergence compared to Jacobi-DD. SSOR-DD also encounters this issue, but the results are not shown here due to space constraints. This problem arises from the biased nature of (7a) for GS/SSOR, as the signal power is not normalized before performing the demodulation in (7b). Consequently, it is crucial to normalize the signal power in order to ensure consistency between these two steps.

B. Normalized-SI Methods

Theorem 2: Given $\mathbf{A} = \mathbf{H}^H \mathbf{H}$, the signal power for each data stream in SI-methods can be normalized to 1 by replacing (7a) as follows

$$\mathbf{s}_t = \mathbf{d}_{t-1} + (\mathbf{M}\mathbf{U})^{-1}(\mathbf{b} - \mathbf{A}\mathbf{d}_{t-1}), \tag{11}$$

where $\mathbf{U}$ represents the diagonal part of $[\mathbf{M}^{-1}\mathbf{A}]$.

Proof: See Appendix B. ∎

By employing (11) instead of (7a), the proposed methods can be referred to as NGS/NSSOR. It is worth noting that the signal power for the Jacobi iteration is already normalized to

one, and inline with *Theorem 1*. The performance comparison illustrated in Fig. 1 demonstrates that NGS-DD outperforms GS-DD in terms of both convergence rate and SER performance. When comparing NGS-DD and Jacobi-DD, it becomes evident that NGS-DD has a faster convergence rate, while Jacobi-DD shows better SER performance. Consequently, the subsequent section aims to combine the advantages of both methods.

C. ANPID Method with Pseudocode

In this section, by alternating use NGS/NSSOR-DD and Jacobi-DD methods, two types of ANPID methods are proposed: ANPID (GS) and ANPID (SSOR). The ANPID methods comprise two stages, specifically Stage A and Stage B, and their iterative process can be expressed as:

$$\mathbf{s}_t = \mathbf{d}_{t-1} + \boldsymbol{\Theta}(\mathbf{b} - \mathbf{A}\mathbf{d}_{t-1}), \tag{12a}$$

$$\mathbf{x}_t = \Gamma\left(\mathbf{s}_t\right), \tag{12b}$$

$$\mathbf{d}_t = \zeta \mathbf{d}_{t-1} + (1 - \zeta)\mathbf{x}_t, \tag{12c}$$

where $\boldsymbol{\Theta}$ and ζ represent the alternative preconditioning matrix and damping factor, respectively. The value of $\boldsymbol{\Theta}$ and ζ will be alternated between Stage A and Stage B. For instance, in the case of ANPID (GS) method, NGS-DD is utilized in Stage A for fast convergence, where $\boldsymbol{\Theta} = (\mathbf{M}_{\text{GS}}\mathbf{U})^{-1}$ and $\zeta_A = \omega_{\text{GS}}$. Subsequently, in Stage B, Jacobi-DD is implemented for close-to-MLSD performance, where $\boldsymbol{\Theta} = \mathbf{D}^{-1}$ and $\zeta_B = \omega_{\text{JAC}}$. The pseudocode of ANPID (GS) method is shown below:

Algorithm ANPID (GS) Method

Input:
  $\mathbf{A}$; $\mathbf{b}$; $\mathbf{M}_{\text{GS}}$; $\mathbf{d}_0 = \mathbf{0}$; T_A/T_B: iterations of Stage A/B
Output:
  $\mathbf{x}_t$: the decision vector;
START
1: **let** $t = 1$, $\boldsymbol{\Theta} = (\mathbf{M}_{\text{GS}}\mathbf{U})^{-1}$; call (12a) (12b) to compute $\mathbf{x}_1$, $\mathbf{z}_1$;
    call (10) to compute $\omega_{\text{GS}}^\star$ and $\omega_{\text{Jac}}^\star$;
    let $\zeta = \omega_{\text{GS}}^\star$, call (12c) to compute $\mathbf{d}_1$; $t \leftarrow t + 1$;
2: **while** $t \leq T_A$;
    call (12) to compute $\mathbf{s}_t$, $\mathbf{x}_t$, and $\mathbf{d}_t$; $t \leftarrow t + 1$;
3: **let** $\boldsymbol{\Theta} = \mathbf{D}^{-1}$; $\zeta = \omega_{\text{Jac}}^\star$;
4: **while** $t \leq T_A + T_B$;
    call (12) to compute $\mathbf{s}_t$, $\mathbf{x}_t$, and $\mathbf{d}_t$; $t \leftarrow t + 1$;
END

The damping factors (i.e., $\omega_{\text{GS}}^\star$ and $\omega_{\text{Jac}}^\star$) can be computed using (10), respectively. When implementing this algorithm, ANPID (GS) is able to offer fast convergence and close-to-MLSD performance simultaneously, as illustrated in Fig. 1 with $T_A = 3$. By replacing $\mathbf{M}_{\text{GS}}$ with $\mathbf{M}_{\text{SSOR}}$, the above algorithm can be adapted to become ANPID (SSOR).

D. Complexity Analysis

In this section, the computational complexity of the proposed methods is analyzed and compared with that of existing techniques. The preprocessing of $\mathbf{A}$ and $\mathbf{b}$ is not considered, as it is common to all current MIMO detectors and can be parallelized.
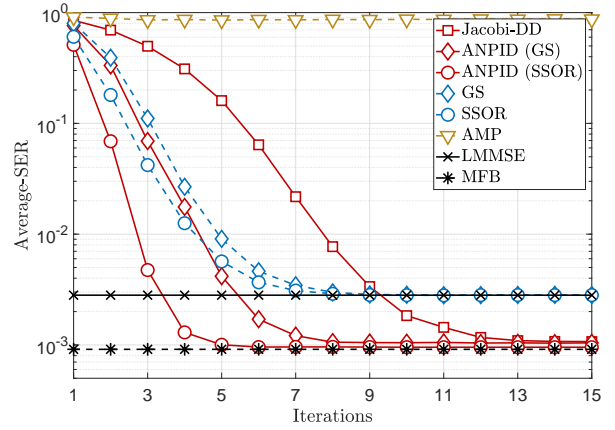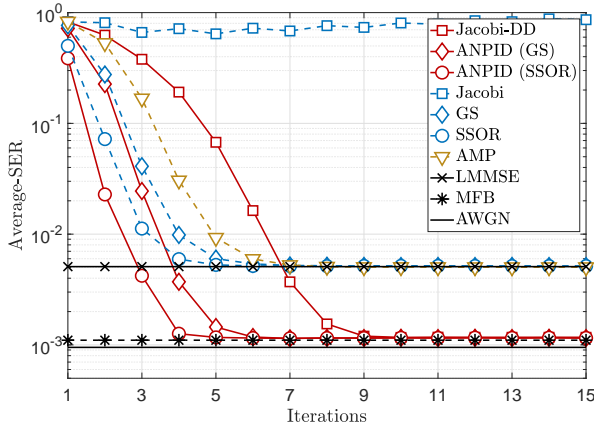
Fig. 2. SER versus iteration in 256×64 large-MIMO systems with 64 QAM and $T_A = 3$. The three proposed methods can offer close-to-AWGN performance. **Left:** WSSUS channel; Es/No = 24 dB. **Right:** ELAA channel; Es/No = 31 dB.

TABLE I
COMPARISON OF COMPLEXITY AND PERFORMANCE FOR DIFFERENT MIMO DETECTORS

Algorithm	Serial Complexity	Parallel Complexity (Per Iteration)		Best Performance
		$t = 1$	$t \geq 2$	
Jacobi Iteration	0	N	N^2	LMMSE
GS Iteration	N^2	$0.5N^2$	$1.5N^2$	LMMSE
SSOR	N^2	N^2	$2N^2$	LMMSE
AMP	0	$2MN$	$2MN$	LMMSE
PS-ADMM	N^3	MN	N^2	Better than LMMSE
Jacobi-DD	0	$2MN$	N^2	Close-to-MLSD
ANPID (GS)	N^2	$0.5N^2 + 2MN$	$1.5N^2 \rightarrow N^2$	Close-to-MLSD
ANPID (SSOR)	N^2	$N^2 + 2MN$	$2N^2 \rightarrow N^2$	Close-to-MLSD

For ANPID (GS), the serial complexity of computing $\mathbf{M}_{GS}^{-1}$ is $\mathcal{O}(N^2)$, owing to the triangular structure of $\mathbf{M}_{GS}$. The remaining calculations in ANPID (GS) can be executed in parallel. The computation cost of $\mathbf{U}$ in the first iteration is $0.5N^2$, while calculating ω_{GS} and ω_{Jac} according to (10) has a complexity of $MN + 3M$. In Stage A, the complexity of computing $\boldsymbol{\Theta}(\mathbf{b} - \mathbf{A}\mathbf{d}_{t-1})$ is $1.5N^2$, which reduces to $N^2 + N$ in Stage B. The complexity of $\Gamma(\mathbf{s}_t)$ is negligible, as it involves no multiplication. Finally, the complexity of damping process in (12c) is $2N$. As for ANPID (SSOR), the serial complexity of computing $\mathbf{M}_{SSOR}^{-1}$ is also $\mathcal{O}(N^2)$, because $\mathbf{M}_{SSOR}^{-1} = (\mathbf{M}_{GS}^H)^{-1}\mathbf{D}\mathbf{M}_{GS}^{-1}$. The other components of ANPID (SSOR) are similar to those of ANPID (GS).

TABLE I presents a comparison between the proposed MIMO detectors and existing techniques in terms of both complexity and performance. To conserve space, the linear complexities have been excluded from the table since they have a negligible impact on the overall complexity of the MIMO detectors. The table shows that existing MIMO detectors with square-order complexities can only provide LMMSE performance, while nonlinear MIMO detectors such as PS-ADMM can offer better than LMMSE performance, but at a cubic-order complexity. In contrast, only the proposed methods (i.e., Jacobi-DD, ANPID (GS), and ANPID (SSOR)) can achieve close-to-MLSD performance with square-order complexities. Jacobi-DD is capable of fully parallel computation, while ANPID (GS) and ANPID (SSOR) exhibit faster

convergence rates among these methods.

IV. SIMULATION RESULTS

In this section, computer simulations are conducted in both WSSUS and ELAA channels. To ensure a fair comparison, we set $\mathbf{x}_0 = \mathbf{0}$ and $\mathbf{d}_0 = \mathbf{0}$ for all the methods. It is computational prohibitive to perform MLSD with large N in Monte Carlo simulations. Therefore, we use the performance of AWGN channel as the lower bound for WSSUS channel, and the matched filter bound (MFB) as the performance lower-bound for ELAA channels. Denote $\mathbf{x}_{MFB}$ as the decision of MFB, it can be expressed as follows [17]

$$\mathbf{x}_{MFB} = \Gamma(\mathbf{s} + \mathbf{D}^{-1}\mathbf{v}), \tag{13}$$

where $\mathbf{D}$ denotes the diagonal part of $[\mathbf{H}^H\mathbf{H}]$. In MFB, it is assumed that the interference is perfectly eliminated, and then maximum ratio combining is used for each interference-free data stream. Therefore, MFB can serve as a performance lower bound for MIMO detectors. For large-MIMO systems deployed with an ELAA, the service-antennas are deployed in a large uniform linear array (ULA) with half-wavelength equal spacing at a central frequency of 3.5 GHz. The perpendicular distance between the ELAA and the users is set to be 15 meters. According to [3], the system parameters are set as follows: $\alpha = 0.020$, $\beta = 1.765$, and $\sigma_s = 6.053$. Three experiments are conducted in this section.

Experiment 1: The objective of this experiment is to evaluate the detection performance and convergence rate of various methods. In Fig. 2, we present the SER versus iteration for both WSSUS and ELAA channels. There is a considerable performance gap between LMMSE and MFB in both channels, which implies that all the linear MIMO detectors can only offer sub-optimal performance. In WSSUS channels, the original Jacobi iteration fails, since the ratio of N/M is too large [18]. When comparing ANPID (GS) to GS or AUPID (SSOR) to SSOR, it becomes apparent that the former has a faster convergence rate. This is because ANPID methods incorporate a damping demodulation step into SI methods, which helps to improve convergence speed. As shown in
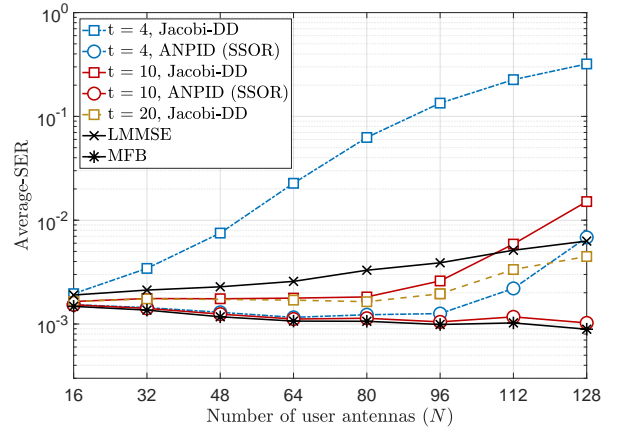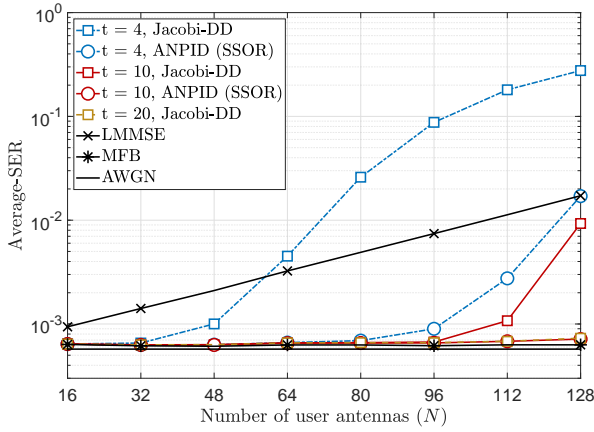
Fig. 3. SER versus N with M fixed at 256 using 16 QAM modulation; $T_A = 3$. It is demonstrated that the detection performance of the proposed methods are scalable as N increases. **Left:** WSSUS channel; Es/No = 18 dB. **Right:** ELAA channel; Es/No = 27 dB.
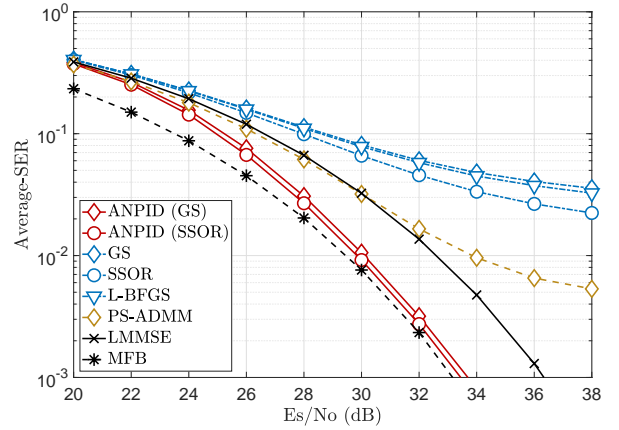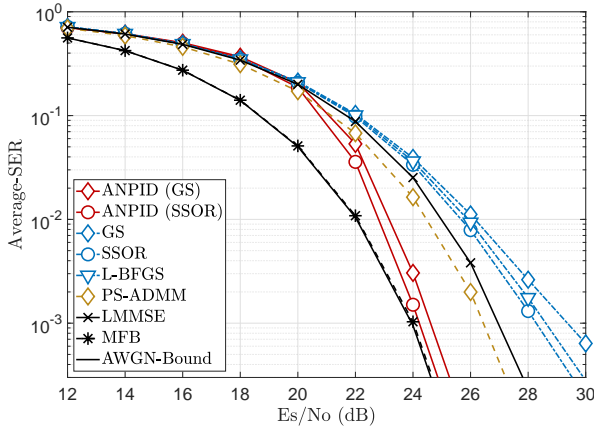

Fig. 4. SER versus Es/No in highly-loaded large-MIMO systems with $M = 256$ and $N = 128$; 64 QAM; $T_A = 5$. The proposed ANPID methods can provide a performance gain of around 3 dB when the SER is approximately 10^{-3}. **Left:** WSSUS channel. **Right:** ELAA channel.

the figure, only the three proposed methods (i.e., Jacobi-DD, ANPID (GS), and ANPID (SSOR)) are capable of achieving close-to-MLSD performance in both WSSUS and ELAA channels. It is observed that ANPID (SSOR) has the fastest convergence rate, whereas Jacobi-DD takes advantage of its ability to support fully parallel computation despite having a slower convergence rate. In the ELAA channel, all iterative methods exhibit slower convergence rates compared to that in WSSUS channels, due to the channels spatial non-stationarity. Furthermore, it is evident that the AMP algorithm fails due to the channel spatial non-stationarity, while the proposed methods remain robust to ELAA channels and still offer close-to-MLSD performance. Remarkably, for ANPID (SSOR) methods, very similar convergence rate (i.e., converging at $t = 5$) is achieved in both WSSUS and ELAA channels.

Experiment 2: This experiment aims to demonstrate the scalability of the proposed methods in terms of detection performance as N increases, while M is fixed. The results in Fig. 3 show that ANPID (SSOR) and Jacobi-DD both provide close-to-AWGN performance in WSSUS channels. This indicates that the performance using the proposed methods remains almost constant as the system load increases. In ELAA channels, Jacobi-DD does not offer close-to-MFB

performance (while AUPID (SSOR) does), but it still outperforms LMMSE. The increasing inter-symbol interference in highly-loaded large-MIMO systems causes the performance gap between LMMSE and AWGN to widen. This implies that all low-complexity algorithms that can only offer LMMSE detection performance will be too sub-optimal in such systems. In contrast, the results in Fig. 3 indicate that ANPID methods can achieve close-to-MLSD while maintaining low computational complexity and fast convergence, which is crucial for practical large-MIMO systems.

Experiment 3: The purpose of this experiment is to evaluate the detection performance of the proposed methods in different levels of Es/No. As shown in Fig. 4, the SER versus Es/No is plotted for various MIMO detectors in both WSSUS and ELAA channels. The ANPID methods, compared to LMMSE, can provide a performance gain of about 3 dB in both stationary and non-stationary MIMO channels, when SER is at 10^{-3}. It is notable that the performance gain between ANPID methods and LMMSE is greater at high Es/No ranges, which is typically the working range of large-MIMO systems. In addition, the results show that PS-ADMM can only offer better-than-LMMSE performance in WSSUS channels. However, PS-ADMM is no longer able to outperform LMMSE in ELAA

channels. On the other hand, ANPID methods demonstrate robustness to the spatial non-stationarity of ELAA channels.

V. Conclusion

In this paper, three iterative algorithms for large-MIMO detection were developed: Jacobi-DD, ANPUD (GS), and ANPID (SSOR). The ANPID methods were shown to have faster convergence than Jacobi-DD, albeit with slightly higher complexity, and all methods can achieve close-to-MLSD performance with square-order complexity. The simulation results showed that the proposed ANPID methods outperformed LMMSE by approximately 3 dB in highly-loaded large-MIMO systems, which indicates that half of the transmit power can be saved in the physical layer. The scalability and performance of the proposed methods make them suitable for practical use in modern wireless communication systems. Finally, it is worth mentioning that the proposed methods are not limited to large-MIMO detection only, but can also be utilized to solve integer least squares problems in other domains, such as signal processing and computer vision.

Appendix A
Proof of *Theorem* 1

Similar to the objective of MLSD in (4), it is proposed to calculated ω_t by minimizing the Euclidean distance between $\mathbf{y}$ and $[\mathbf{Hd}_t]$ as follows

$$\omega_t = \arg\min_{\omega_t}\|\mathbf{y} - \mathbf{Hd}_t\|^2. \qquad (14)$$

Plugging (7c) into (14) yields

$$\omega_t = \arg\min_{\omega_t}\|\mathbf{y} - \mathbf{Hx}_t - \omega_t(\mathbf{Hd}_{t-1} - \mathbf{Hx}_t)\|^2,$$
$$= \arg\min_{\omega_t}\|\boldsymbol{\tau}_t - \omega_t\boldsymbol{\nu}_t\|^2, \qquad (15)$$

which is a quadratic function on ω_t. Let $\frac{\partial}{\partial\omega}\|\boldsymbol{\tau}_t - \omega_t\boldsymbol{\nu}_t\|^2 = 0$, (8) in *Theorem 1* can be obtained.

Appendix B
Prove of Theorem 2

Eqn. (11) in *Theorem 2* can be reformulated as follows

$$\mathbf{s}_t = (\mathbf{I} - (\mathbf{MU})^{-1}\mathbf{A})\mathbf{d}_{t-1} + (\mathbf{MU})^{-1}\mathbf{b}. \qquad (16)$$

Define $\mathbf{F} \triangleq (\mathbf{MU})^{-1}\mathbf{A}$, and plugging $\mathbf{b} = \mathbf{H}^H\mathbf{y}$ and $\mathbf{y} = \mathbf{Hx} + \mathbf{v}$ into (16) yields

$$\mathbf{s}_t = (\mathbf{I} - \mathbf{F})\mathbf{d}_{t-1} + (\mathbf{MU})^{-1}\mathbf{H}^H(\mathbf{Hx} + \mathbf{v}),$$
$$= \mathbf{Fx} + (\mathbf{I} - \mathbf{F})\mathbf{d}_{t-1} + (\mathbf{MU})^{-1}\mathbf{H}^H\mathbf{v}, \qquad (17)$$

where the first two terms can be reformulated as follows

$$\mathbf{Fx} + (\mathbf{I} - \mathbf{F})\mathbf{d}_{t-1} = \mathbf{Fx} - \mathbf{x} + \mathbf{x} + (\mathbf{I} - \mathbf{F})\mathbf{d}_{t-1},$$
$$= \mathbf{x} + (\mathbf{I} - \mathbf{F})(\mathbf{d}_{t-1} - \mathbf{x}). \qquad (18)$$

Plugging (18) into (17) yields

$$\mathbf{s}_t = \mathbf{x} + (\mathbf{I} - \mathbf{F})(\mathbf{d}_{t-1} - \mathbf{x}) + (\mathbf{MU})^{-1}\mathbf{H}^H\mathbf{v}, \qquad (19)$$

where the first term is the normalized signal vector. From the definitions of $\mathbf{F}$ and $\mathbf{U}$, it is clear that the diagonal elements of $\mathbf{F}$ are all equal to 1. Consequently, $[\mathbf{I} - \mathbf{F}]$ is a hollow matrix, meaning the second term in (18) contains only inter-symbol interference. Furthermore, the third term corresponds to the noise vector and does not contain any signal component. This confirms the validity of the expression derived in *Theorem 2*.

References

[1] M. Cui, Z. Wu, Y. Lu, X. Wei, and L. Dai, "Near-field MIMO communications for 6G: Fundamentals, challenges, potentials, and future directions," *IEEE Commun. Mag.*, vol. 61, no. 1, pp. 40–46, Jan. 2023.

[2] E. Björnson, L. Sanguinetti, H. Wymeersch, J. Hoydis, and T. L. Marzetta, "Massive MIMO is a reality–What is next? Five promising research directions for antenna arrays," *Digit. Signal Process.*, vol. 94, pp. 3–20, Nov. 2019.

[3] J. Liu, Y. Ma, J. Wang, N. Yi, R. Tafazolli, S. Xue, and F. Wang, "A non-stationary channel model with correlated NLoS/LoS states for ELAA-mMIMO," in *Proc. IEEE Global Commun. Conf. (GLOBECOM)*, 2021, pp. 1–6.

[4] S. Yang and L. Hanzo, "Fifty years of MIMO detection: The road to large-scale MIMOs," *IEEE Commun. Surveys Tuts.*, vol. 1, no. 4, pp. 1941–1988, 4th Quart. 2015.

[5] M. A. Albreem, M. Juntti, and S. Shahabuddin, "Massive MIMO detection techniques: A survey," *IEEE Commun. Surveys Tuts.*, vol. 21, no. 4, pp. 3109–3132, 4th Quart. 2019.

[6] Z. Chen and E. Björnson, "Channel hardening and favorable propagation in cell-free massive MIMO with stochastic geometry," *IEEE Trans. Commun.*, vol. 66, no. 11, pp. 5205–5219, Nov. 2018.

[7] J. Liu, Y. Ma, and R. Tafazolli, "Leveraging user-wise SVD for accelerated convergence in iterative ELAA-MIMO detections," in *Proc. IEEE 24th Int. Workshop Signal Process. Advances Wireless Commun. (SPAWC)*, 2023.

[8] M. A. Albreem, A. H. Alhabbash, S. Shahabuddin, and M. Juntti, "Deep learning for massive MIMO uplink detectors," *IEEE Commun. Surveys Tuts.*, vol. 24, no. 1, pp. 741–766, 1st Quart. 2022.

[9] S. Shahabuddin, I. Hautala, M. Juntti, and C. Studer, "ADMM-based infinity-norm detection for massive MIMO: Algorithm and VLSI architecture," *IEEE Trans. VLSI Syst.*, vol. 29, no. 4, pp. 747–759, Feb. 2021.

[10] I. N. Tiba, Q. Zhang, J. Jiang, and Y. Wang, "A low-complexity ADMM-based massive MIMO detectors via deep neural networks," in *Proc. IEEE Int. Conf. Acoust. Speech Signal Process. (ICASSP)*, 2021, pp. 4930–4934.

[11] Q. Zhang, J. Wang, and Y. Wang, "Efficient QAM signal detector for massive MIMO systems via PS/DPS-ADMM approaches," *IEEE Trans. Wireless Commun.*, vol. 21, no. 10, pp. 8859–8871, Oct. 2022.

[12] J.-C. Chen, "A low complexity data detection algorithm for uplink multiuser massive MIMO systems," *IEEE J. Sel. Areas Commun.*, vol. 35, no. 8, pp. 1701–1714, Jun. 2017.

[13] M. Hochwald, T. L. Marzetta, and V. Tarokh, "Multiple-antenna channel hardening and its implications for rate feedback and scheduling," *IEEE Trans. Inf. Theory*, vol. 50, no. 9, pp. 1893–1909, Sep. 2004.

[14] J. Liu, Y. Ma, and R. Tafazolli, "Achieving maximum-likelihood detection performance with square-order complexity in large quasi-symmetric MIMO systems," in *Proc. IEEE Int. Symp. Inf. Theory (ISIT)*, 2023.

[15] C. Zhang, Z. Wu, C. Studer, Z. Zhang, and X. You, "Efficient soft-output Gauss–Seidel data detector for massive MIMO systems," *IEEE Trans. Circuits Syst. I*, vol. 68, no. 12, pp. 5049–5060, Dec. 2021.

[16] T. Xie, L. Dai, X. Gao, X. Dai, and Y. Zhao, "Low-complexity SSOR-based precoding for massive MIMO systems," *IEEE Commun. Lett.*, vol. 20, no. 4, pp. 744–747, Apr. 2016.

[17] A. Amiri, S. Rezaie, C. N. Manchón, and E. de Carvalho, "Distributed receiver processing for extra-large MIMO arrays: A message passing approach," *IEEE Trans. Wireless Commun.*, vol. 21, no. 4, pp. 2654–2667, Apr. 2022.

[18] Z. Wang, R. M. Gower, Y. Xia, L. He, and Y. Huang, "Randomized iterative methods for low-complexity large-scale MIMO detection," *IEEE Trans. Signal Process.*, vol. 70, pp. 2934–2949, Jun. 2022.